Histone H3.3K27M Mobilizes Multiple Cancer/Testis (CT) Antigens in Pediatric Glioma

Houliang Deng[1], Jianming Zeng[1], Ting Zhang[1], Longcai Gong[1], Hongjie Zhang[1], Edwin Cheung[1], Chris Jones[2], Gang Li[1]

[1]Faculty of Health Sciences, University of Macau, Macau, China. [2]Centre for Evolution and Cancer, Divisions of Molecular Pathology and Cancer Therapeutics, the Institute of Cancer Research, Sutton, SM2 5NG, UK.

Running Title: Histone H3.3K27M Activates C/T Antigens

Key Words: Pediatric Gliomas, Mutation, Histone H3, Cancer-testis antigens, Immunotherapy

Corresponding Author:

Gang Li, Ph.D.

Assistant Professor

Faculty of Health Sciences, University of Macau

E12-3014, Avenida da Universidade, Taipa, Macau, China

Tel: +853-8822-4212

Fax: +853-8822-2314

E-mail: gangli@umac.mo

Disclosure of Potential Conflicts of Interest: None

Abstract

Lysine to Methionine mutations at position 27 (K27M) in the histone H3 (H3.3 and H3.1) are highly prevalent in pediatric high-grade gliomas (HGG) that arise in the midline of the central nervous system. H3K27M perturbs the activity of polycomb repressor complex 2 (PRC2) and correlates with DNA hypomethylation; however, the pathways whereby H3K27M drive the development of pediatric HGG remain poorly understood. To understand the mechanism of pediatric HGG development driven by H3.3K27M and discover potential therapeutic targets or biomarkers, we established pediatric glioma cell model systems harboring H3.3K27M and performed microarray analysis. H3.3K27M caused the upregulation of multiple cancer/testis (CT) antigens, such as ADAMTS1, ADAM23, SPANXA1, SPANXB1/2, IL13RA2, VCY and VCX3A, in pediatric glioma cells. Chromatin immunoprecipitation (ChIP) analysis from H3.3K27M cells revealed decreased H3K27me3 levels and increased H3K4me3 levels on the VCX3A promoter. Knockdown of VCX3A by siRNA significantly inhibited the growth of pediatric glioma cells harboring H3.3K27M. Overexpression of VCX3A/B genes stimulated the expression of several human leukocyte antigens (HLA) genes, including HLA-A, HLA-B, HLA-E, HLA-F, and HLA-G. The expression of VCX3A in pediatric HGG was confirmed using a tissue microarray. Gene set enrichment analysis (GSEA) revealed CT antigens are enriched in pediatric HGG clinical specimens with H3.3K27M, with the upregulation of IL13RA2 contributing to the enrichment significantly. These results indicate that the upregulation of CT antigens, such as VCX3A and IL13RA2, correlates with pediatric gliomagenesis.

Introduction

Brain and central nervous system (CNS) tumors are the leading causes of cancer-related death and the second most common cancers in children and adolescents aged birth to 19 years old (1). Among various childhood brain tumors, pediatric high-grade gliomas (HGG) is the deadliest type. Even with a combination of the most advanced treatments, few patients achieve long-term survival (1). Thus, understanding the molecular mechanisms of pediatric HGG and developing new therapeutic agents for pediatric HGG is of prime importance. Recently, epigenetic changes, mutations in or altered expression of epigenetic machinery have been implicated in the development of various cancers including pediatric HGG (2,3). Significantly, sequencing of pediatric HGG tumors revealed the c.83A>T mutations in H3F3A or HIST1H3B/C, which result in the lysine 27 to methionine (K27M) missense mutations in histone H3.3 or H3.1 respectively (4-6). The H3K27M mutations are enriched in pediatric HGG residing in the midline structures, such as pontine, brainstem, thalamus and spinal cord (7-12). Significantly, ~80 % of pediatric diffuse intrinsic pontine gliomas (DIPG) harbor the H3K27M mutations (4-6,13). H3K27M mutations were also detected in adult HGG, albeit at a much lower frequency (14,15), indicating there are substantial differences in the genetic and epigenetic mechanisms underlying the development of pediatric and adult HGG.

Because the H3K27M mutation is highly prevalent in pediatric HGG and occurs at the target site of polycomb repressive complex 2 (PRC2), the discovery attracted considerable attention. Follow-up investigations showed that H3K27M held the PRC2 activity in check, and behaved dominant-negatively and caused a global decrease of the H3K27me3 level (16,17). DNA hypomethylation (decreased 5-methylcytosine) was observed in pediatric HGG by multiple studies (13,18-22). A global reduction of the H3K27me3 level and DNA hypomethylation potentially act together to drive gliomagenesis, however, the detailed mechanisms whereby H3K27M drive gliomagenesis remains poorly understood.

Cancer/testis (CT) antigens are characterized by a unique class of tumor antigens, which are aberrantly expressed in a wide variety of tumors and are silent in normal tissues, except for

the immune privileged male germ cells (23-26). Due to their tumor-restricted pattern of expression and robust immunogenicity, CT antigens are considered to be ideal targets for cancer biomarkers and immunotherapy. So far, more than 250 CT antigens have been identified (27). VCX/Y (Variable charge, X-linked/Y-linked) genes, which are primate-specific genes and encode positively charged proteins of largely unknown function, are newly identified CT antigens in lung cancers (28). VCX/Y family proteins include six members, VCX3A, VCX, VCX2, VCX3B, VCY and VCY1B. They share a highly homologous N-terminal region, and their C-terminal regions are composed of different numbers of copies of a ten-amino-acid repeat. The X-linked members are organized in tandem on a region of chromosome Xp22 and interspersed by other genes; the region could undergo non-allelic homologous recombination (NAHR) and other complex rearrangements, potentially resulting in X-linked ichthyosis and cognitive impairment (29-31).

In this study, we found H3.3K27M could activate the expression of multiple CT antigens in pediatric glioma cells, and demonstrated that IL13RA2, and members of the variable charge X/Y (VCX/Y) gene family, were among the top upregulated genes in glioma cells stably expressing H3.3K27M. We further performed functional analysis of VCX3A/B, analyzed the epigenetic configurations at the VCX3A gene region, investigated the effects of VCX3A/B overexpression on the gene expression profiles of glioma cells and examined the expression of VCX3A in pediatric glioma samples. In addition, we performed the gene set enrichment analysis (GSEA) using available data, and revealed H3K27M could indeed activate the expression of CT antigens in clinical samples.

Materials and Methods

Cell culture

Pediatric glioma cell line SF188 was obtained from Dr. Daphne Haas-Kogan (UCSF, San Francisco, CA), and Res259 were obtained from Dr. Michael Bobola (University of Washington, Seattle, WA). Both cell lines are cultured in high glucose Dulbecco's Modified Eagle Medium growth media (Gibco #11965) supplemented with 10% fetal bovine serum. Cells were authenticated by short tandem repeat (STR) profiling (The Institute of Cancer Research, UK) (32) and tested negative for mycoplasma contamination using MycoAlert™ Mycoplasma Detection Kit (Lonza).

Generation of stable cell lines

Human H3F3A (C-terminal Myc-DDK-tagged) cloned into the pCMV6-Entry was purchased from OriGene. The H3.3K27M (c.83A>T) mutation was introduced by the QuikChange Lightning Site-Directed Mutagenesis Kit (Agilent Technologies) according to the manufacturer's protocol. Different isoforms of VCX3A/B were amplified using cDNA derived from Res259 cells as a template and cloned into pcDNA3 GFP LIC cloning vector (6D), which was a gift from Scott Gradia (Addgene plasmid # 30127). SF188 and Res259 cells were transfected using the Lipofectamine 2000 transfection reagent (Invitrogen, #11668019). 1 mg/mL geneticin (G418, Thermo Fisher Scientific) was added to the culture medium for selecting stably transfected clones. The corresponding empty expression vectors were stably transfected into cells to serve as controls.

Cell proliferation and apoptosis assays

2×10^3 cells were plated in 96-well plates in 100 µl medium. Cell proliferation was analyzed by the CellTiter-Glo® luminescent cell viability assay (Promega) for five consecutive days. For apoptosis assay, cells were grown to 70–80 % confluence, then harvested and stained using the Annexin V-FITC Apoptosis Detection Kit (Beyotime) and then analyzed by an FACScan flow

cytometer (BD Biosciences). The data were analyzed with the FlowJo software (Treestar).

5-Methylcytosine (5-mC) dot blot assay

Genomic DNA was isolated with the DNeasy Blood & Tissue Kit (Qiagen #69506), denatured in 0.4 M NaOH, 10 mM EDTA at 95 °C for 10 min, then neutralized with cold 2 M ammonium acetate (pH 7.0). Two-fold serial dilutions of the denatured DNA samples were spotted onto a nitrocellulose membrane using the Bio-Dot apparatus (Bio-Rad). The membrane was washed with 2x saline-sodium citrate (SSC) buffer, air-dried and cross-linked by UV irradiation, then blocked with 5% non-fat milk for 1 hour and incubated with anti-5mC (Active Motif #39649, 1:10000) overnight at 4 °C. The membrane was visualized by enhanced chemiluminescence after incubating with HRP-conjugated anti-mouse IgG secondary antibody. The same blot was subsequently stained with 0.01% methylene blue to verify equal loading.

Total RNA isolation

Total RNA was extracted using the TRIzol reagent (Invitrogen), and genomic DNA was digested by RNase-Free DNase Set (QIAGEN, #79254), the RNA was further purified using the RNeasy Mini Kit (Qiagen, #74106) following manufacturer’s instructions. Quality and concentration of RNA were determined by the Bioanalyzer 2100 (Agilent technologies).

Gene expression analysis

Total RNA was amplified and labeled using the TargetAmp™-Nano Labeling Kit for Illumina Expression BeadChip (Epicentre Biotechnologies, #TAN091096). Labeled cRNA was purified with the RNeasy mini kit (QIAGEN, #74106) and hybridized on HumanHT-12 v4 Expression BeadChip microarrays (Illumina) according to the manufacturer's protocol. The hybridized arrays were scanned using the Illumina iScan (Illumina), and the image data were extracted using the Illumina GenomeStudio software. The raw data were deposited in the Gene Expression Omnibus data repository with accession number GSE102886.

Quantitative real-time reverse transcription PCR

1 μg of total RNA was used to synthesize the cDNA using the SuperScript® III First-Strand Synthesis System (Invitrogen). Quantitative PCR (qPCR) was carried out using the LightCycler® 480 SYBR Green I Master (Roche) in the CFX 96 thermocycler (Bio-Rad). The assays were performed in triplicate and repeated three times. The relative expression level of the gene of interest was normalized to GAPDH, and calculated according to the 2^{-ddCt} method (33). The primers used in this study can be found in the Supplementary Table S1.

Chromatin immunoprecipitation (ChIP)

Chromatin immunoprecipitation (ChIP) was performed using the EZ-Magna ChIP™ A/G Chromatin Immunoprecipitation Kit (Millipore #17-10086) following the manufacturer's instruction. Briefly, cells were cross-linked with 1% formaldehyde and sonicated to obtain DNA fragments between 0.3 and 1.0 kb. Chromatin was incubated with anti-H3K27me3 (Millipore #07-449), anti-H3K4me3 (Millipore #07-473) antibodies, and normal rabbit IgG (Cell signal technology #2729S) overnight and the immune complexes were precipitated by protein A/G magnetic beads. DNA was extracted and used for ChIP-qPCR analysis. The enrichment levels are presented as percentage of input chromatin.

Western blot

Total protein was extracted using RIPA buffer supplemented with proteinase inhibitor cocktail (Sigma-Aldrich). The extracted proteins were separated by SDS-PAGE and then transferred to nitrocellulose membrane (Pall Corporation). Membranes were blocked with 5% non-fat milk and then incubated with the following antibodies: anti-FLAG (Sigma #F1804), anti-H3K27me3 (Millipore #07-449), anti-H3K4me3 (Millipore #07-473), anti-Histone H3 (Abcam #ab1791), anti-Histone H3 (K27M mutant, Millipore #ABE419), anti-VCX3A (Abnova, #H00051481-M01), anti-GAPDH (Cell Signaling, #5174S), anti-β-actin (Santa Cruz Biotechnology, sc-47778).

Membranes were then incubated with horseradish peroxidase-conjugated secondary antibodies (Jackson ImmunoResearch), and the signals were detected by the Supersignal West Pico Chemiluminescent Substrate (Thermo Fisher Scientific).

VCX3A knockdown by siRNA

Two siRNAs targeting VCX3A (siVCX #1: Hs_VCX_8 FlexiTube siRNA, #SI04173568, and siVCX #2: Hs_VCX_10 FlexiTube siRNA, cat. #SI04187295; Qiagen) were transfected independently into cells at a final concentration of 25 nM using Lipofectamine RNAiMAX (Life Technologies) per the manufacturer's instruction. 48 hours after transfection, total RNA and protein were harvested for analysis, and the CellTiter-Glo® Luminescent Cell Viability Assay (Promega) was performed in triplicate for three independent experiments to examine cell growth.

DNA methylation analysis

Total genomic DNA was isolated from Res259 cells using the DNeasy Blood & Tissue Kit (Qiagen, #69506). The genomic DNA was subjected to bisulfite conversion using the EpiTect Bisulfite Kit (Qiagen, #59104). Primers targeting VCX3A or GAPDH for bisulfite-sequencing were designed by MethPrimer (34) and the primer sequences are listed in the Supplementary Table S1. The bisulfite-modified DNA was amplified via PCR and cloned into the T-Vector pMD20 (Takara, #3270). The plasmid DNA was sequenced to determine the CpG methylation status. Only sequences with higher than 99.5% bisulfite conversion rate were included in the analysis.

Immunohistochemical analysis

Tissue microarrays comprising 43 pediatric HGG were collated at the Institute of Cancer Research (London, UK) from multiple collaborating centers, all under approval from local ethical research committees. The slides were deparaffinized and hydrated, and antigen retrieval was performed using the 2100 retriever (Aptum Biologics) in R-Buffer A (pH 6.0). Intrinsic peroxidase activity was blocked using 3% hydrogen peroxide for 5 minutes. Slides were then incubated with

the antibody against human VCX3A (Abnova #H00051481-M01, 1:50) overnight at 4℃; then the slides were stained using the SuperPicture™ 3rd Gen IHC Detection Kit (Thermo Fisher Scientific) according to the manufacturer's protocol.

Gene set enrichment analysis (GSEA)

Publicly available pediatric HGG gene expression profiles (GSE34824, GSE36245, GSE49822) were downloaded from Gene Expression Omnibus (https://www.ncbi.nlm.nih.gov/geo/). The raw data were processed with Robust Multi-array Average (RMA) (35) background correction and quantile normalization, combined and stratified for H3F3A status (H3F3A K27M (K27M), n = 14; H3F3A wild-type (WT), n = 51) per the published sample annotation, then subjected to the analysis. Gene set enrichment analysis (GSEA) was performed using GSEA software (version 3.0) (36,37). The signature gene set consists of the full list of cancer-testis (CT) antigens deposited in CTdatabase (http://www.cta.lncc.br/), including 276 genes. The custom Gene Matrix Transposed (GMT) file containing the list of CT antigens that we constructed for GSEA analysis is attached as supplementary data.

Results

H3.3K27M reduces the global level of tri-methylation of H3K27

To determine the effects of H3.3K27M mutation on gliomagenesis in vitro, we first established two pediatric glioma cell lines stably carrying the mutation. Constructs encoding a FLAG-tagged wild-type (WT) or K27M mutant form of histone H3.3 were stably transfected into pediatric glioma cells, Res259 (WHO grade II) or SF188 (WHO grade IV) cells, whereas the empty vector was stably transfected into cells to serve as controls. Consistent with previous studies (16,17), H3.3K27M significantly reduced the global levels of H3K27me3 in both cell lines, while did not affect the global levels of H3K4me3 (Fig. 1A). A modest reduction of global DNA methylation level was also observed by 5-mC dot blot assay in two independent clones of Res259 cells harboring the H3.3K27M mutation (Fig. 1B), consistent with the reduction of DNA methylation found in clinical pediatric glioma samples with the H3.3K27M mutation (13,18-22). However, exogenous expression of H3.3K27M did not have an apparent effect on the cell proliferation and apoptosis in both cell lines (Fig. 1C & D).

H3.3K27M significantly upregulates multiple cancer/testis antigens

To gain insight into the molecular mechanisms underlying gliomagenesis driven by H3.3K27M, microarray analysis was carried out on Res259 with or without the K27M mutation. 290 genes were found to be differentially expressed between Res259-K27M and Res259-vector control cells, of which 84 genes were downregulated (log2 fold change < - 0.5, $P < 0.05$) and 206 genes upregulated in Res259-K27M cell (log2 fold change > 0.5, $P < 0.05$) (Fig. 2A). KEGG (Kyoto Encyclopedia of Genes and Genomes) analysis (38) revealed that the upregulated genes were enriched in pathways including transcriptional misregulation in cancer, MAPK signaling, cell cycle, p53 signaling, ErbB signaling, and Hippo signaling; whereas the down-regulated genes were enriched in pathways including AMPK, metabolism, PPAR, and calcium signaling (Fig. 2B). Intriguingly, we found that 12 of the top 50 upregulated genes in cells with H3.3K27M are cancer/testis (CT) antigens (Figure 2C). To validate the observations, the mRNA levels of

selected CT antigens were examined by RT-qPCR in two independent H3.3K27M expressing Res259 stable clones. As shown in Fig. 3A, H3.3K27M mutation significantly induced the expression of ADAM metallopeptidase domain 23 (ADAM23), ADAM metallopeptidase with thrombospondin type 1 motif 1 (ADAMTS1), interleukin 13 receptor subunit alpha 2 (IL13RA2), sperm protein associated with the nucleus, X-linked, family member A1, B1/B2 (SPANXA1, SPANXB1/2), variable charge, X-linked 3A (VCX3A) and variable charge, Y-linked (VCY) in Res259 cells, when compared to control cells stably transfected with the empty vector. A similar trend was also observed in SF-188 cells expressing H3.3K27M (Supplementary Fig. S1A). Significantly, it seems that positive stimulation of expression of CT antigens is K27M specific since ectopic expression of wild-type Histone H3 (H3.3WT) could not cause a similar change (Fig. 3A and Fig. S1A). Among the CT antigens upregulated in H3.3K27M carrying cells, genes of variable charge X/Y family, such as VCX3A and VCY, had the highest fold changes of expression. In addition, overexpression of VCX3A in H3.3K27M carrying cells could be confirmed at the protein level by Western blot analysis (Fig. 3B and Supplementary Fig. S1B). Therefore, we next focused on examining the potential involvement of VCX3A in gliomagenesis.

H3.3K27M alters the epigenetic modifications of VCX3A genomic locus

To get an insight into the mechanisms by which H3.3K27M causes the upregulation of VCX3A expression, we first examined the changes of the epigenetic configurations of the VCX3A genomic locus as a function of H3.3K27M mutation. By chromatin immunoprecipitation coupled with quantitative PCR (ChIP-qPCR), we found the level of H3K4me3 on the promoter of VCX3A increased, and the level of H3K27me3 on the promoter of VCX3A decreased in the Res259 cells harboring H3.3K27M (Fig. 4B).

Previous studies reported that H3.3K27M could not only cause the reduction of global H3K27me3 level, but also DNA hypomethylation (13,18,19). Thus, we next examined the DNA methylation status at the VCX3A locus of the Res259 cells. By bioinformatics analysis, we found there were no CpG islands (CGIs) at the promoter of all four VCX genes. Instead, there were

CGIs in the gene bodies of VCX genes (Supplementary Fig. S2). We performed bisulfite sequencing targeting an intragenic CGI of VCX3A, which overlaps with the exon 2 of VCX3A (Fig. 4A). Surprisingly, we observed an increased DNA methylation at this CGI in the cells carrying H3.3K27M compared to empty vector transfected control (Figure 4C), while no changes of DNA methylation status were found in an intragenic CGI of the housekeeping gene GAPDH (Supplementary Fig. S3). Methylation of intragenic CpG islands (iCGIs) is reported to be positively correlated with gene transcription by unclear mechanisms (39,40). Hypermethylation of the iCGI of VCX3A indicates the correlation between gene activation and methylation of iCGI remains intact in the mutant cells, and the observed hypermethylation of the iCGI of VCX3A might be a consequence of active VCX3A transcription. Together, these results support the changed epigenetic landscape caused by H3.3K27M was associated the upregulation of VCX3A.

Knockdown of VCX3A inhibits cell growth

We next set out to knock down VCX3A in Res259 (WHO grade II) and SF188 (WHO grade IV) cells harboring H3.3K27M to explore their function. Two siRNAs (Qiagen) were used to target VCX3A gene. Due to high similarity of VCX/Y family genes, Hs_VCX_8 FlexiTube siRNA (siVCX #1) targets all the VCX/Y genes, whereas Hs_VCX_10 FlexiTube siRNA (siVCX #2) targets VCX3A, VCX3B and VCX, but not VCX2 and VCY. As shown in Fig. 5A, both siRNAs could knock down VCX3A efficiently. The knockdown of VCX3A significantly inhibited the proliferation of the two cell lines carrying the K27M mutation (Fig. 5B). However, the cell growth inhibitory effect could not be observed in Res259 cells without the K27M mutation (Fig. 5B), which could be explained by the low expression of VCX3A in the vector control Res259 cells. In all, these results suggested that VCX3A might play an oncogenic role in pediatric HGG.

VCX3A/B overexpression stimulates the expression of human leukocyte antigens (HLA)

To perform functional analysis of VCX3A, we next set out to clone the VCX3A gene from the

cDNA of Res259. We designed primers targeting the coding region of VCX3A, however, because the coding region of VCX3A and VCX3B have identical 5' and 3' ends, the primers we used also targeting VCX3B unavoidably. Indeed, DNA sequencing revealed that three genes we cloned bearing N-termini identical to the N-terminus of VCX3A (NCBI Ref Seq: NM_016379.3), which are followed by 10, 7 or 2 copies of a ten-amino acid repeat respectively, at their C-termini (Fig. 6A). Surprisingly, the composition and organization of the C-termini of the genes share higher similarity to VCX3B (NCBI Ref Seq: NM_001001888.3) than to VCX3A (Supplementary file 1), suggesting VCX gene family locus is polymorphic and subject to alternative splicing or recombination. However, further studies are required to clarify the precise mechanisms involved. In this study, we distinguished the VCX family genes we cloned by the number of the tandem repeats they bear, and named them as VCX3A/B-10R, VCX3A/B-7R and VCX3A/B-2R, due to their resemblance to a hybrid of the reference sequences of VCX3A and VCX3B. Next, we generated Res-259 cells stably expressing different isoforms of VCX3A/B fused with GFP. Consistent with the presence of a putative bipartite nuclear localization sequence (KRKSSSQPSPSDPKKKTT) at the N-terminus of VCX3A/B, all three isoforms of GFP-VCX3A/B were observed to be primarily localized to the nucleus (Supplementary Fig. S4), suggesting that VCX3A/B members are nuclear proteins.

To understand the function of VCX3A/B proteins and their potential involvement in gliomagenesis, we next examined the changes of gene expression profiles caused by VCX3A/3B overexpression by microarray analysis. Briefly, RNA was extracted from Res259 cells stably expressing the different isoforms of VCX3A/B-GFP, or GFP control, and subjected to an Illumina HT12.2 Bead CHIP array analysis. As shown in Fig. 6B and Supplementary Fig. S5, the different isoforms of VCX3A/B caused similar gene expression changes. Therefore, the data sets were combined for subsequent analysis. 138 genes were found to be differentially expressed in VCX3A/B overexpressing Res259 cells compared to GFP-control cells, of which 35 genes were downregulated (log2 fold change < - 0.5, $P < 0.05$) and 103 genes were upregulated in Res259-VCX3A/B cells (log2 fold change > 0.5, $P < 0.05$). Gene ontology analysis revealed that

the upregulated genes in VCX3A/B overexpressing cells are primarily involved in immune response. Significantly, VCX3A/B overexpression caused the upregulation of major histocompatibility complex (MHC) class I genes, including HLA-A, HLA-B, HLA-E, HLA-F and HLA-G (Fig. 6D & 6E). MHC class I molecules are primarily involved in binding to and presenting antigens on the cell surface for recognition by cytotoxic T cells. Upregulation of MHC class I molecules by VCX3A/B suggests VCX3A/B proteins are processed by MHC class I proteins in cells. We further examined the expression of HLA genes in Res259 cells carrying the H3.3K27M mutation by RT-qPCR. Indeed, minor upregulations of HLA genes, particularly of the HLA-B, were observed in cells carrying H3.3K27M (supplementary Fig. S6).

The expression of VCX3A and other CT antigens in pediatric HGG.

We next examined the expression of VCX3A protein with tissue microarrays comprising 43 pediatric and young adult HGG. VCX3A showed primarily nuclear staining and was strongly expressed in normal testis but was negative in normal brain (Fig. 7A). Of three samples harboring H3.3K27M, one showed strong expression of VCX3A, one showed moderate expression and the third showed negative/equivocal expression. Among the forty tumors with wild-type Histone H3, one showed strong expression of VCX3A (2.5%), and three showed moderate expression (7.5%) (Fig. 7A & 7B, Supplementary Table S2), indicating the expression of VCX3A was not limited to tumors carrying the H3K27M mutation and other mechanisms also potentially activates the expression of VCX3A in pediatric HGG.

To further examine whether H3.3K27M mutation could activate CT antigens, we collected and combined the published microarray datasets of pediatric HGG deposited in the Gene Expression Omnibus (GEO) repository of NCBI, which include 14 samples with H3.3K27M mutation, and 51 samples with wild-type H3.3 (5,13,18). We next performed Gene Set Enrichment Analysis (GSEA) using the full list of CT antigens curated in the CTdatabase (http://www.cta.lncc.br) as the Gene Matrix, which contains 276 genes (27). As shown in Fig. 7C, CT antigens are enriched in tumors with H3.3K27M mutation compared with those without the

mutation with an enrichment score 0.38 (*P* = 0.037; FDR q-value = 0.159), indicating the activation of CT antigens might be one of the hallmarks of pediatric HGG harboring H3.3K27M. Notably, interleukin 13 receptor alpha 2 (IL13RA2), which have been explored as a therapeutic target for adult glioblastoma (41), is one of the top upregulated CT antigens in pediatric HGG with H3.3K27M (Fig. 7D).

Discussion

In this study, we found that H3.3K27M could activate the expression of multiple cancer/testis (CT) antigens. Among them, VCX/Y family, which were recently proposed as novel CT antigens in lung cancers (28,42), were the most upregulated. VCX/Y genes are specific to primates and absent from non-primate mammals. Expression of members of the VCX/Y gene family is restricted to testis. VCX/Y gene family contains four paralogues (VCX3A, VCX, VCX2 and VCX3B) on X chromosome and two paralogues (VCY, VCY1B) on Y chromosome. Their functions remain largely unknown. Deletion of VCX3A was observed in X-linked nonspecific mental retardation patients (29,31). Jiao et al. found that VCX3A bound the 5' end of capped mRNAs to prevent mRNA decapping and decay (43), and inhibit mRNA translation (44). The author further proposed that VCX3A modulates neuritogenesis through selective binding to mRNAs (44). Also, the enrichment of VCX/Y in nucleoli and the putative interaction of VCX3A with RPLP0 (Ribosomal Protein Lateral Stalk Subunit P0) also suggest their potential involvement in ribosome biogenesis (45). Consistent with the results in lung cancer, we observed knockdown of VCX3A inhibited the growth of the pediatric glioma cells harboring H3.3K27M, suggesting its potential involvement in gliomagenesis. However, more detailed studies are needed to validate the proposed functions of VCX3A and explore the unknown.

The expression of CT antigens is regulated epigenetically by DNA methylation within the promoter region and histone modifications (23,24,46,47). Perhaps, the strongest evidence for the involvement of epigenetics in the regulation of CT antigens come from the induction of the expression of CT antigens by chemical inhibitors of DNA methylation, or inhibitors of histone deacetylases and histone methyltransferases (23,24,46,47). In this study, we provided evidence that the changed epigenetic landscape contributes to the upregulation VCX3A in the cells carrying H3.3K27M. Tissue microarray-based analysis showed that VCX3A was expressed in pediatric HGG, but the expression was not limited only to tumors harboring H3.3K27M, suggesting multiple pathways are involved in activation of VCX3A. The H3.3K27M mutation could cause the global reduction of H3K27me3 and DNA hypomethylation (13,16-19,21,22), both

of which would potentially affect the expression of CT antigens. Consequently, other than VCX/Y, we also observed the overexpression of CT antigens including ADAMTS1, ADAM23, SPANXA1, SPANXB1/2, and IL13RA2 in pediatric glioma cells carrying H3.3K27M.

In general, CT antigens are digested by the proteasome into small peptides, then transported into the endoplasmic reticulum (ER), and presented on the cell surface by major histocompatibility complex (MHC) class I molecules. Mutations in or downregulation of MHC class I molecules are the mechanisms most frequently exploited by tumor cells to escape from immune surveillance (48). In this study, we found overexpression of VCX3A/B in pediatric glioma cells strongly stimulates the expression of HLA-A, HLA-B, HLA-E, HLA-F and HLA-G, indicating VCX3A/B are probably presented by the MHC class I mediated pathway as antigens. Once VCX3A/B are presented, the tumor cells bearing them could potentially be recognized and eliminated by the host immune system. This could explain the observation that, although H3.3K27M activates the expression of VCX/Y in cell culture models, only part of the clinical samples with H3.3K27M have VCX/Y overexpression. However, the underlying mechanisms of upregulation of MHC molecules driven by VCX3A/B and its potential significance remain to be explored.

Immunotherapeutic approaches for treating brain tumors, including pediatric gliomas, have been actively explored (49-51). For example, a trial using the H3.3K27M peptide as a vaccine for the treatment of HLA-A2+ H3.3K27M positive gliomas is ongoing (NCT02960230). Considering testis does not express MHC class I or II molecules and therefore being immune-privileged, CT antigens are proposed to be ideal targets for cancer immunotherapy because of the tumor-restricted pattern of expression and their strong immunogenicity in vivo (23,26). Accordingly, clinical trials have utilized CT antigens as targets for adoptive T-cell therapy, or as vaccines against tumors, including gliomas (24,25,41,52). Significantly, an adult glioblastoma patient had tumor regression after receiving chimeric antigen receptor (CAR)-engineered T cells targeting IL13RA2 (41). In this study, we observed the upregulation of IL13RA2 in pediatric glioma cells carrying H3.3K27M, and further confirmed its upregulation in pediatric HGG with

H3.3K27M using published datasets.

In summary, we found that H3.3K27M could cause upregulation of multiple CT antigens in pediatric glioma cells, including IL13RA2 and VCX3A/B. Our data also indicate VCX3A/B might be oncogenic. Thus, it is worth exploring the potential use of VCX3A/B and IL13RA2 as immunotherapeutic targets for pediatric HGG.

Acknowledgments

The authors thank the iPSC Core of the University of Macau and Professor Guokai Chen for help with the mycoplasma detection assay. Grant Support: This work was supported by the Science and Technology Development Fund of Macau [137/2014/A3, 095/2015/A3] and the Research & Development Administration Office of the University of Macau [SRG201400015, MYRG201500232, MYRG201700099].

References

1. Ward E, DeSantis C, Robbins A, Kohler B, Jemal A. Childhood and adolescent cancer statistics, 2014. CA: a cancer journal for clinicians **2014**;64(2):83-103 doi 10.3322/caac.21219.
2. Liu KW, Pajtler KW, Worst BC, Pfister SM, Wechsler-Reya RJ. Molecular mechanisms and therapeutic targets in pediatric brain tumors. Science signaling **2017**;10(470) doi 10.1126/scisignal.aaf7593.
3. Lulla RR, Saratsis AM, Hashizume R. Mutations in chromatin machinery and pediatric high-grade glioma. Science advances **2016**;2(3):e1501354 doi 10.1126/sciadv.1501354.
4. Khuong-Quang D-A, Buczkowicz P, Rakopoulos P, Liu X-Y, Fontebasso AM, Bouffet E*, et al.* K27M mutation in histone H3.3 defines clinically and biologically distinct subgroups of pediatric diffuse intrinsic pontine gliomas. Acta neuropathologica **2012**;124(3):439-47 doi 10.1007/s00401-012-0998-0.
5. Schwartzentruber J, Korshunov A, Liu XY, Jones DT, Pfaff E, Jacob K*, et al.* Driver mutations in histone H3.3 and chromatin remodelling genes in paediatric glioblastoma. Nature **2012**;482(7384):226-31 doi 10.1038/nature10833.
6. Wu G, Broniscer A, McEachron TA, Lu C, Paugh BS, Becksfort J*, et al.* Somatic histone H3 alterations in pediatric diffuse intrinsic pontine gliomas and non-brainstem glioblastomas. Nature genetics **2012**;44(3):251-3 doi 10.1038/ng.1102.
7. Aihara K, Mukasa A, Gotoh K, Saito K, Nagae G, Tsuji S*, et al.* H3F3A K27M mutations in thalamic gliomas from young adult patients. Neuro-oncology **2014**;16(1):140-6 doi 10.1093/neuonc/not144.
8. Venneti S, Santi M, Felicella MM, Yarilin D, Phillips JJ, Sullivan LM*, et al.* A sensitive and specific histopathologic prognostic marker for H3F3A K27M mutant pediatric glioblastomas. Acta neuropathologica **2014**;128(5):743-53 doi 10.1007/s00401-014-1338-3.

9. Zhang L, Chen LH, Wan H, Yang R, Wang Z, Feng J*, et al.* Exome sequencing identifies somatic gain-of-function PPM1D mutations in brainstem gliomas. Nature genetics **2014**;46(7):726-30 doi 10.1038/ng.2995.
10. Feng J, Hao S, Pan C, Wang Y, Wu Z, Zhang J*, et al.* The H3.3 K27M mutation results in a poorer prognosis in brainstem gliomas than thalamic gliomas in adults. Hum Pathol **2015** doi 10.1016/j.humpath.2015.07.002.
11. Gessi M, Gielen GH, Dreschmann V, Waha A, Pietsch T. High frequency of H3F3A (K27M) mutations characterizes pediatric and adult high-grade gliomas of the spinal cord. Acta neuropathologica **2015**;130(3):435-7 doi 10.1007/s00401-015-1463-7.
12. Pathak P, Jha P, Purkait S, Sharma V, Suri V, Sharma MC*, et al.* Altered global histone-trimethylation code and H3F3A-ATRX mutation in pediatric GBM. Journal of neuro-oncology **2015**;121(3):489-97 doi 10.1007/s11060-014-1675-z.
13. Sturm D, Witt H, Hovestadt V, Khuong-Quang DA, Jones DT, Konermann C*, et al.* Hotspot mutations in H3F3A and IDH1 define distinct epigenetic and biological subgroups of glioblastoma. Cancer cell **2012**;22(4):425-37 doi 10.1016/j.ccr.2012.08.024.
14. Reyes-Botero G, Giry M, Mokhtari K, Labussiere M, Idbaih A, Delattre JY*, et al.* Molecular analysis of diffuse intrinsic brainstem gliomas in adults. Journal of neuro-oncology **2014**;116(2):405-11 doi 10.1007/s11060-013-1312-2.
15. Reuss DE, Sahm F, Schrimpf D, Wiestler B, Capper D, Koelsche C*, et al.* ATRX and IDH1-R132H immunohistochemistry with subsequent copy number analysis and IDH sequencing as a basis for an "integrated" diagnostic approach for adult astrocytoma, oligodendroglioma and glioblastoma. Acta neuropathologica **2015**;129(1):133-46 doi 10.1007/s00401-014-1370-3.
16. Chan KM, Fang D, Gan H, Hashizume R, Yu C, Schroeder M*, et al.* The histone H3.3K27M mutation in pediatric glioma reprograms H3K27 methylation and gene expression. Genes & development **2013**;27(9):985-90 doi 10.1101/gad.217778.113.
17. Lewis PW, Muller MM, Koletsky MS, Cordero F, Lin S, Banaszynski LA*, et al.* Inhibition of PRC2 Activity by a Gain-of-Function H3 Mutation Found in Pediatric Glioblastoma. Science **2013**;340(6134):857-61 doi 10.1126/science.1232245.
18. Bender S, Tang Y, Lindroth AM, Hovestadt V, Jones DT, Kool M*, et al.* Reduced H3K27me3 and DNA hypomethylation are major drivers of gene expression in K27M mutant pediatric high-grade gliomas. Cancer cell **2013**;24(5):660-72 doi 10.1016/j.ccr.2013.10.006.
19. Saratsis AM, Kambhampati M, Snyder K, Yadavilli S, Devaney JM, Harmon B*, et al.* Comparative multidimensional molecular analyses of pediatric diffuse intrinsic pontine glioma reveals distinct molecular subtypes. Acta neuropathologica **2014**;127(6):881-95 doi 10.1007/s00401-013-1218-2.
20. Buczkowicz P, Bartels U, Bouffet E, Becher O, Hawkins C. Histopathological spectrum of paediatric diffuse intrinsic pontine glioma: diagnostic and therapeutic implications. Acta neuropathologica **2014**;128(4):573-81 doi 10.1007/s00401-014-1319-6.
21. Buczkowicz P, Hoeman C, Rakopoulos P, Pajovic S, Letourneau L, Dzamba M*, et al.* Genomic analysis of diffuse intrinsic pontine gliomas identifies three molecular subgroups and recurrent activating ACVR1 mutations. Nature genetics **2014**;46(5):451-6 doi 10.1038/ng.2936.
22. Ahsan S, Raabe EH, Haffner MC, Vaghasia A, Warren KE, Quezado M*, et al.* Increased 5-hydroxymethylcytosine and decreased 5-methylcytosine are indicators of global epigenetic

dysregulation in diffuse intrinsic pontine glioma. Acta neuropathologica communications **2014**;2:59 doi 10.1186/2051-5960-2-59.

23. Caballero OL, Chen YT. Cancer/testis (CT) antigens: potential targets for immunotherapy. Cancer science **2009**;100(11):2014-21 doi 10.1111/j.1349-7006.2009.01303.x.

24. Fratta E, Coral S, Covre A, Parisi G, Colizzi F, Danielli R*, et al.* The biology of cancer testis antigens: putative function, regulation and therapeutic potential. Molecular oncology **2011**;5(2):164-82 doi 10.1016/j.molonc.2011.02.001.

25. Gjerstorff MF, Andersen MH, Ditzel HJ. Oncogenic cancer/testis antigens: prime candidates for immunotherapy. Oncotarget **2015**;6(18):15772-87 doi 10.18632/oncotarget.4694.

26. Simpson AJ, Caballero OL, Jungbluth A, Chen YT, Old LJ. Cancer/testis antigens, gametogenesis and cancer. Nat Rev Cancer **2005**;5(8):615-25 doi 10.1038/nrc1669.

27. Almeida LG, Sakabe NJ, deOliveira AR, Silva MC, Mundstein AS, Cohen T*, et al.* CTdatabase: a knowledge-base of high-throughput and curated data on cancer-testis antigens. Nucleic Acids Res **2009**;37(Database issue):D816-9 doi 10.1093/nar/gkn673.

28. Taguchi A, Taylor AD, Rodriguez J, Celiktaş M, Liu H, Ma X*, et al.* A search for novel cancer/testis antigens in lung cancer identifies VCX/Y genes, expanding the repertoire of potential immunotherapeutic targets. Cancer Res **2014**;74(17):4694-705 doi 10.1158/0008-5472.can-13-3725.

29. Fukami M, Kirsch S, Schiller S, Richter A, Benes V, Franco B*, et al.* A member of a gene family on Xp22.3, VCX-A, is deleted in patients with X-linked nonspecific mental retardation. Am J Hum Genet **2000**;67(3):563-73 doi 10.1086/303047.

30. Lahn BT, Page DC. A human sex-chromosomal gene family expressed in male germ cells and encoding variably charged proteins. Human molecular genetics **2000**;9(2):311-9.

31. Van Esch H, Hollanders K, Badisco L, Melotte C, Van Hummelen P, Vermeesch JR*, et al.* Deletion of VCX-A due to NAHR plays a major role in the occurrence of mental retardation in patients with X-linked ichthyosis. Human molecular genetics **2005**;14(13):1795-803 doi 10.1093/hmg/ddi186.

32. Bax DA, Little SE, Gaspar N, Perryman L, Marshall L, Viana-Pereira M*, et al.* Molecular and phenotypic characterisation of paediatric glioma cell lines as models for preclinical drug development. PloS one **2009**;4(4):e5209 doi 10.1371/journal.pone.0005209.

33. Livak KJ, Schmittgen TD. Analysis of relative gene expression data using real-time quantitative PCR and the 2(-Delta Delta C(T)) Method. Methods (San Diego, Calif) **2001**;25(4):402-8 doi 10.1006/meth.2001.1262.

34. Li LC, Dahiya R. MethPrimer: designing primers for methylation PCRs. Bioinformatics (Oxford, England) **2002**;18(11):1427-31.

35. Irizarry RA, Hobbs B, Collin F, Beazer-Barclay YD, Antonellis KJ, Scherf U*, et al.* Exploration, normalization, and summaries of high density oligonucleotide array probe level data. Biostatistics **2003**;4(2):249-64 doi 10.1093/biostatistics/4.2.249.

36. Subramanian A, Tamayo P, Mootha VK, Mukherjee S, Ebert BL, Gillette MA*, et al.* Gene set enrichment analysis: a knowledge-based approach for interpreting genome-wide expression profiles. Proceedings of the National Academy of Sciences of the United States of America **2005**;102(43):15545-50 doi 10.1073/pnas.0506580102.

37. Subramanian A, Kuehn H, Gould J, Tamayo P, Mesirov JP. GSEA-P: a desktop application for Gene Set Enrichment Analysis. Bioinformatics (Oxford, England) **2007**;23(23):3251-3 doi

10.1093/bioinformatics/btm369.
38. Kanehisa M, Goto S. KEGG: kyoto encyclopedia of genes and genomes. Nucleic Acids Res **2000**;28(1):27-30.
39. Yang X, Han H, De Carvalho DD, Lay FD, Jones PA, Liang G. Gene body methylation can alter gene expression and is a therapeutic target in cancer. Cancer cell **2014**;26(4):577-90 doi 10.1016/j.ccr.2014.07.028.
40. Lee SM, Lee J, Noh KM, Choi WY, Jeon S, Oh GT*, et al.* Intragenic CpG islands play important roles in bivalent chromatin assembly of developmental genes. Proceedings of the National Academy of Sciences of the United States of America **2017** doi 10.1073/pnas.1613300114.
41. Brown CE, Alizadeh D, Starr R, Weng L, Wagner JR, Naranjo A*, et al.* Regression of Glioblastoma after Chimeric Antigen Receptor T-Cell Therapy. The New England journal of medicine **2016**;375(26):2561-9 doi 10.1056/NEJMoa1610497.
42. Djureinovic D, Hallstrom BM, Horie M, Mattsson JS, La Fleur L, Fagerberg L*, et al.* Profiling cancer testis antigens in non-small-cell lung cancer. JCI Insight **2016**;1(10):e86837 doi 10.1172/jci.insight.86837.
43. Jiao X, Wang Z, Kiledjian M. Identification of an mRNA-decapping regulator implicated in X-linked mental retardation. Mol Cell **2006**;24(5):713-22 doi 10.1016/j.molcel.2006.10.013.
44. Jiao X, Chen H, Chen J, Herrup K, Firestein BL, Kiledjian M. Modulation of neuritogenesis by a protein implicated in X-linked mental retardation. J Neurosci **2009**;29(40):12419-27 doi 10.1523/JNEUROSCI.5954-08.2009.
45. Zou SW, Zhang JC, Zhang XD, Miao SY, Zong SD, Sheng Q*, et al.* Expression and localization of VCX/Y proteins and their possible involvement in regulation of ribosome assembly during spermatogenesis. Cell Res **2003**;13(3):171-7 doi 10.1038/sj.cr.7290161.
46. Pfister SX, Ashworth A. Marked for death: targeting epigenetic changes in cancer. Nature reviews Drug discovery **2017**;16(4):241-63 doi 10.1038/nrd.2016.256.
47. Van Tongelen A, Loriot A, De Smet C. Oncogenic roles of DNA hypomethylation through the activation of cancer-germline genes. Cancer Lett **2017**;396:130-7 doi 10.1016/j.canlet.2017.03.029.
48. Garrido F, Aptsiauri N, Doorduijn EM, Garcia Lora AM, van Hall T. The urgent need to recover MHC class I in cancers for effective immunotherapy. Current opinion in immunology **2016**;39:44-51 doi 10.1016/j.coi.2015.12.007.
49. Weller M, Roth P, Preusser M, Wick W, Reardon DA, Platten M*, et al.* Vaccine-based immunotherapeutic approaches to gliomas and beyond. Nature reviews Neurology **2017**;13(6):363-74 doi 10.1038/nrneurol.2017.64.
50. Ladomersky E, Genet M, Zhai L, Gritsina G, Lauing KL, Lulla RR*, et al.* Improving vaccine efficacy against malignant glioma. Oncoimmunology **2016**;5(8):e1196311 doi 10.1080/2162402x.2016.1196311.
51. Quail DF, Joyce JA. The Microenvironmental Landscape of Brain Tumors. Cancer cell **2017**;31(3):326-41 doi 10.1016/j.ccell.2017.02.009.
52. Melero I, Gaudernack G, Gerritsen W, Huber C, Parmiani G, Scholl S*, et al.* Therapeutic vaccines for cancer: an overview of clinical trials. Nat Rev Clin Oncol **2014**;11(9):509-24 doi 10.1038/nrclinonc.2014.111.

Figure legends

Figure 1.

Establishing and characterizing cell line models harboring the H3.3K27M mutation. **A,** Pediatric glioma cell lines, SF188 and Res259, were stably transfected with constructs encoding a C-terminal Myc-DDK-tagged wild-type (H3.3WT) form or a Lysine27Methionine (K27M) mutant form of histone H3.3. The parental cell lines (Control) and cells stably transfected with the empty vector (Vector) were used as controls. Acid-extracted histones were subjected to Western blot analysis with the indicated antibodies. **B,** Dot blot analysis using the 5-mC specific antibody to detect global levels of 5-mC on genomic DNA from Res259 cells, which are stably transfected with the empty vector (Vector), or constructs encoding either wild-type Histone H3.3 (H3.3WT), or Histone H3.3 harboring the K27M mutation (K27M). Two independent clones harboring H3.3K27M were examined. Methylene blue staining (bottom panels) was used to assure equal loading. **C,** The CellTiter-Glo® (Promega) luminescent cell viability assays were performed to examine effects of H3.3K27M on cell growth. The assay was conducted in quadruplicate and repeated twice. Error bars represent ± SD of triplicates. **D,** The effects of H3.3K27M on cell apoptosis were examined by annexin V labeling and propidium iodide staining.

Figure 2.

Impacts of H3.3K27M on gene expression in Res259 cells. **A,** Gene expression in Res259 cells were examined by HumanHT-12 v4 Expression BeadChip microarrays (Illumina). The volcano plot shows statistical significance (−log10 *P* value) plotted against log2 fold change of genes for Res259 cells harboring H3.3K27M against vector control cells. Differentially expressed genes (DEGs) were selected by criteria of $P < 0.05$ (blue line) and absolute log2 fold change > 0.5 (red line). **B,** KEGG (Kyoto Encyclopedia of Genes and Genomes) pathway enrichment analysis of DEGs between Res259 cells harboring H3.3K27M and vector control cells. **C,** A pie chart indicates the percentage of cancer/testis (CT) antigens in the top 50 upregulated genes in Res259 cells carrying H3.3K27M as compared to vector control cells.

Figure 3.

H3.3K27M activates cancer/testis (CT)antigens. **A,** mRNA expression of selected CT antigens was examined by RT-qPCR. Res259 cells, which were stably transfected with the empty vector (Vector), or constructs encoding either wild-type Histone H3.3 (H3.3WT) or Histone H3.3 harboring the K27M mutation (K27M) were subjected to experiments. Two independent K27M clones were used to ensure reproducibility. mRNA levels were normalized to GAPDH. Shown are the representatives of three independent experiments. Error bars represent ± standard deviations (SD) of triplicates. ** $P < 0.01$. # A primer set detecting all VCX/Y family genes was used. **B,** Western blot analysis of VCX3A in non-transfected Res259 cells, or Res259 cells stably transfected with the empty vector (control), or constructs encoding wild-type Histone H3.3 (H3.3 WT), or Histone H3.3 harboring the K27M mutation (H3.3K27M). GAPDH was used as a loading control.

Figure 4.

H3.3K27M alters the epigenetic modifications of the VCX3A genomic locus. **A,** A map of the VCX3A gene showing positions of exons (grey rectangles), the intragenic CpG island (CGI, orange diagonal stripes) and two sets of primers (arrows) used for the chromatin immunoprecipitation-qPCR (ChIP-qPCR) analysis. TSS, transcription start site; F, forward primer; R, reverse primer. **B,** Alternations of the indicated histone modification marks on VCX3A genomic locus in Res259 cells carrying H3.3K27M were detected by chromatin immunoprecipitation (ChIP) followed by quantitative real-time PCR. The enrichment of marks is represented by the percent of ChIP input. Res259 cells stably transfected with the empty vector (Vector) served as a control. Left panel: results from primer 1F and 1R; Right panel: results from primers 2F and 2R. *P < 0.05, ** $P < 0.01$; Student's t-test. Error bars represent ± standard deviations (SD) of triplicates. **C,** Increased DNA methylation of an intragenic CpG island (CGI) of VCX3A in Res259 cells carrying H3.3K27M. DNA methylation patterns were determined by

bisulfite sequencing. Res259 cells stably transfected with the empty vector served as a control. Black and white circles represent methylated and unmethylated cytosines, respectively.

Figure 5.

Knockdown of VCX3A inhibits cell growth. **A,** Knockdown of VCX3A with siRNAs in Res259-H3.3K27M and SF188-H3.3K27M cells. The knockdown effects were examined by RT-qPCR (left panels) and Western blot analysis (right panels). GAPDH was used as a loading control. siControl, Negative Control siRNA (Qiagen); siVCX #1, Hs_VCX_8 FlexiTube siRNA; siVCX #2, Hs_VCX_10 FlexiTube siRNA (Qiagen). $^{**}P < 0.01$. **B,** The effects of VCX3A knockdown on cell growth. Cells were transfected with negative control siRNA or two independent siRNAs against VCX3A. 48 hours after transfection, cell growth was examined by CellTiter-Glo kit (Promega) in quadruplicate. Three independent experiments were performed, and results are presented as RLU (relative luminescence unit) fold change compared with the value measured in cells transfected with control siRNA. The cell type is indicated at the top of each graph. $^{**}P < 0.01$.

Figure 6.

A, Diagrams of VCX3A/B genes cloned from Res259 cells. The ten amino acid repeats with different variations are color coded. The genes were named VCX3A/B-10R, VCX3A/B-7R and VCX3A/B-2R respectively, according to the number of repeats (R) they have. **B,** Gene expression changes caused by VCX3A/B expression in Res259 cells were examined by HumanHT-12 v4 Expression BeadChip microarrays (Illumina). The volcano plot shows statistical significance (−log10 *P* value) plotted against log2 fold change of genes for Res259 cells expressing different isoforms of VCX3A/B-GFP versus cells overexpressing GFP alone. The downregulated genes are colored in blue (log2 fold change < −0.5, $P < 0.05$), the upregulated genes are colored in red (log2 fold change > 0.5, $P < 0.05$). **C,** Gene ontology analysis of differentially expressed genes between RES259 cells expressing VCX3A/B-GFP and GFP only.

D, Heatmap of upregulated genes in VCX3A/B overexpressing Res259 cells involved in antigen processing and presentation of endogenous peptide antigen via MHC class I (GO:0002474). **E,** The mRNA expression levels of HLA-A, -B, E, F and G in Res259 cells ectopically expressing different isoforms of VCX3A/B-GFP (2R, 7R and 10R) were evaluated by RT-qPCR, compared to cells expressing GFP alone. Shown are a representative of three independent experiments, error bars represent ± standard deviations (SD) of triplicates. $^{**}P < 0.01$.

Figure 7.

The expression of VCX3A and other CT antigens in pediatric HGG. **A,** Immunohistochemistry for VCX3A protein in pediatric high-grade gliomas (HGG). The tissue microarrays were stained using SuperPicture™ 3rd Gen IHC Detection Kit (Thermo Fisher Scientific). Cell nuclei were counterstained with Hematoxylin. The genotype of H3F3A was indicated on the top of each panel. WT: wild-type; K27M: histone H3 lysine27methionine mutation. Scale bar = 50 μm. **B,** The bar plot of VCX3A expression in pediatric HGG stratified by H3F3A status, depicting the percentage of cases with the indicated signal grades. -, negative; +/-, equivocal; +, weak positive; ++, strong positive. **C,** Gene set enrichment analysis (GSEA) of a signature gene set for cancer/testis (CT) antigens in pediatric HGG with H3F3AK27M mutation versus those with wild-type H3F3A. The signature gene set consists of the full list of CT antigens curated in CTdatabase (http://www.cta.lncc.br/). Publicly available pHGG gene expression profiles (GSE34824, GSE36245, GSE49822) were processed using RMA (quantile normalization), combined and stratified for H3F3A status (H3F3A K27M (K27M), $n = 14$; H3F3A wild-type (WT), $n = 51$) per the published sample annotation, then subjected to the analysis. The normalized enrichment score (NES), the nominal *P* value (NOM p-val) and the false discovery rate *Q* value (FDR q-val) are shown at the upper right corner of the graph. **D,** Upregulation of IL13RA2 in pHGG with the H3.3K27M mutation. The gene expression data of IL13RA2 were retrieved from Gene Expression Omnibus (GEO) of NCBI (GSE34824, GSE36245, GSE49822).

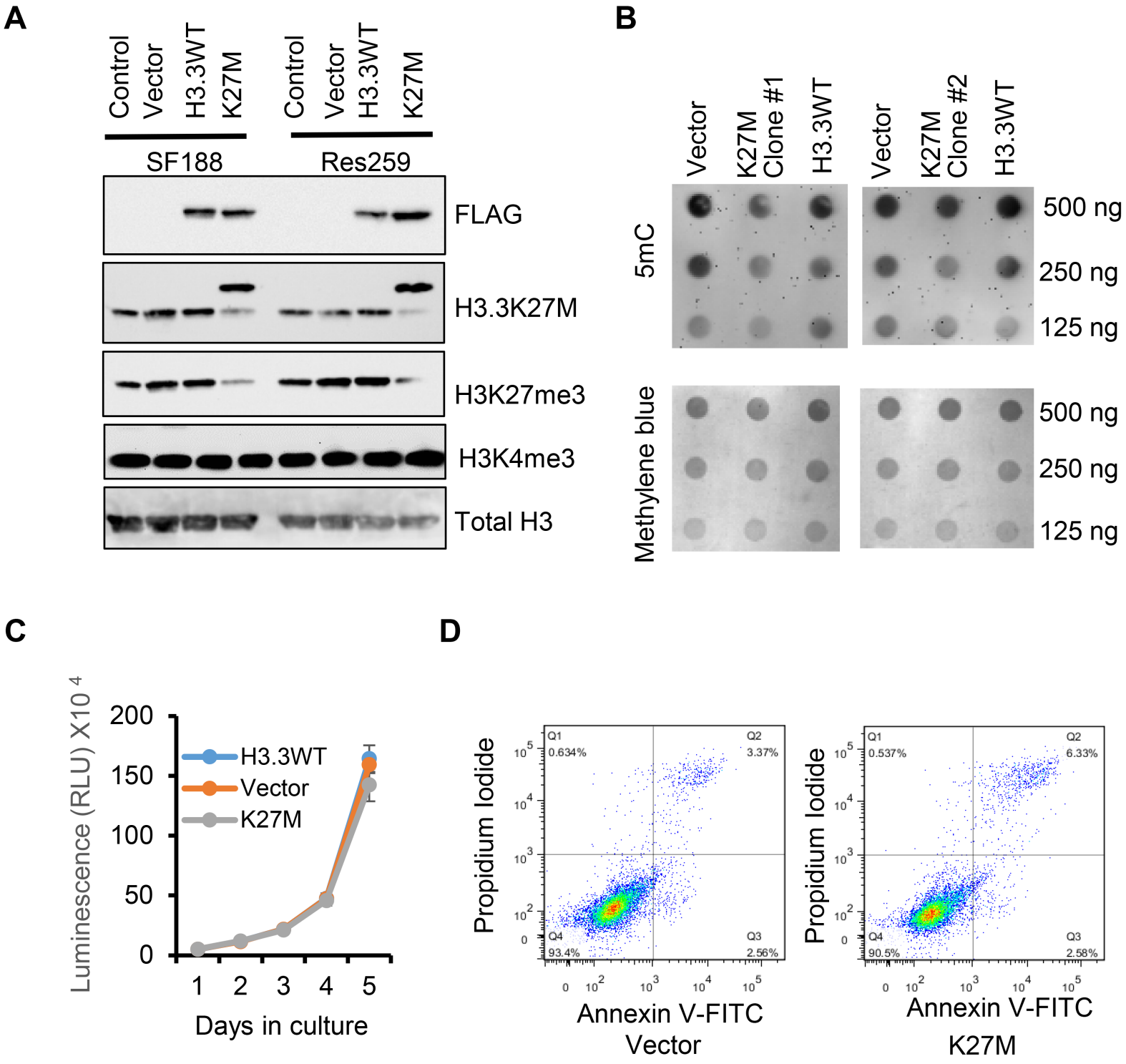
A
Control
Vector
H3.3WT
K27M
Control
Vector
H3.3WT
K27M
SF188
Res259
FLAG
H3.3K27M
H3K27me3
H3K4me3
Total H3
B
Vector
K27M Clone #1
H3.3WT
Vector
K27M Clone #2
H3.3WT
5mC
Methylene blue
500 ng
250 ng
125 ng
500 ng
250 ng
125 ng
C
Luminescence (RLU) X10 4
200
150
100
50
0
H3.3WT
Vector
K27M
1
2
3
4
5
Days in culture
D
Propidium Iodide
Q1
0.634%
Q2
3.37%
Q4
93.4%
Q3
2.56%
Annexin V-FITC
Vector
Propidium Iodide
Q1
0.537%
Q2
6.33%
Q4
90.5%
Q3
2.58%
Annexin V-FITC
K27M

Fig. 1

A

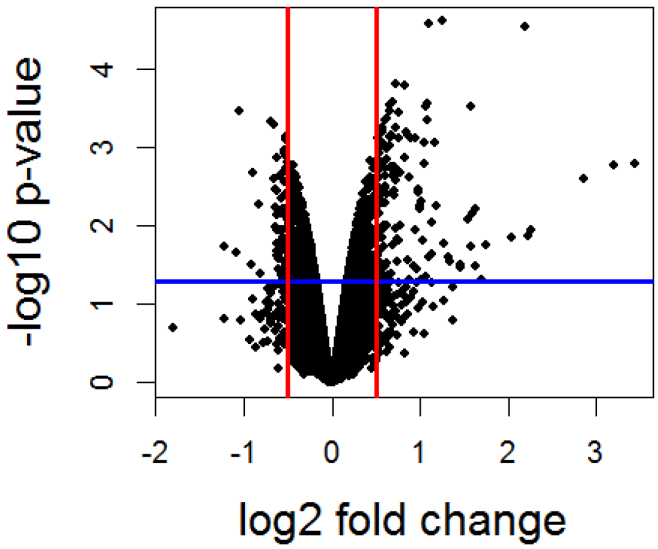
-log10 p-value
0
1
2
3
4
-2
-1
0
1
2
3
log2 fold change

C

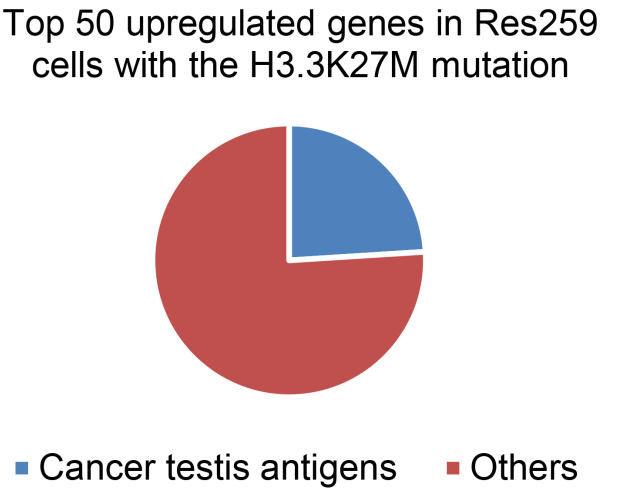
Top 50 upregulated genes in Res259 cells with the H3.3K27M mutation
Cancer testis antigens
Others

B

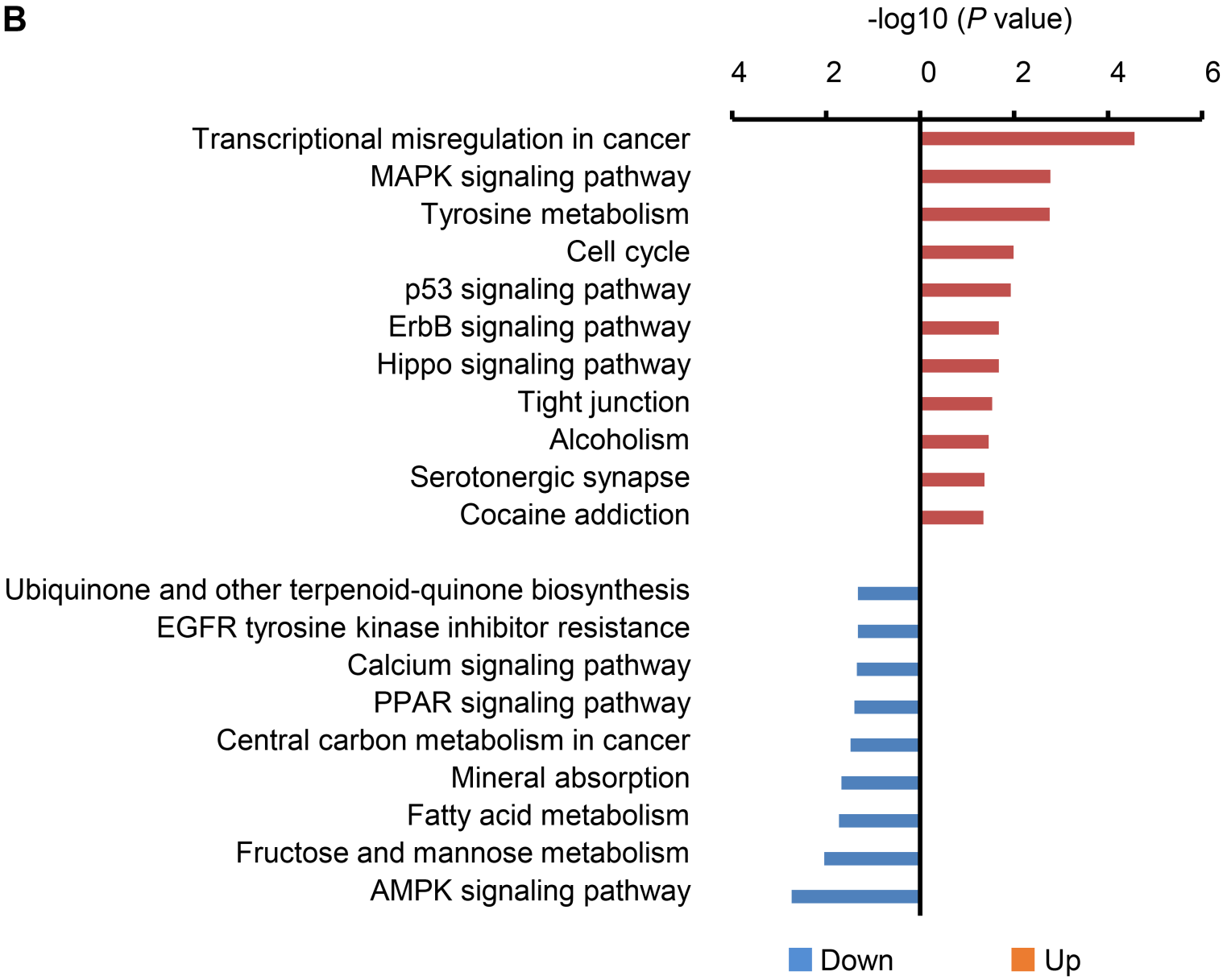
-log10 (P value)
4
2
0
2
4
6
Transcriptional misregulation in cancer
MAPK signaling pathway
Tyrosine metabolism
Cell cycle
p53 signaling pathway
ErbB signaling pathway
Hippo signaling pathway
Tight junction
Alcoholism
Serotonergic synapse
Cocaine addiction
Ubiquinone and other terpenoid-quinone biosynthesis
EGFR tyrosine kinase inhibitor resistance
Calcium signaling pathway
PPAR signaling pathway
Central carbon metabolism in cancer
Mineral absorption
Fatty acid metabolism
Fructose and mannose metabolism
AMPK signaling pathway
Down
Up

Fig. 2

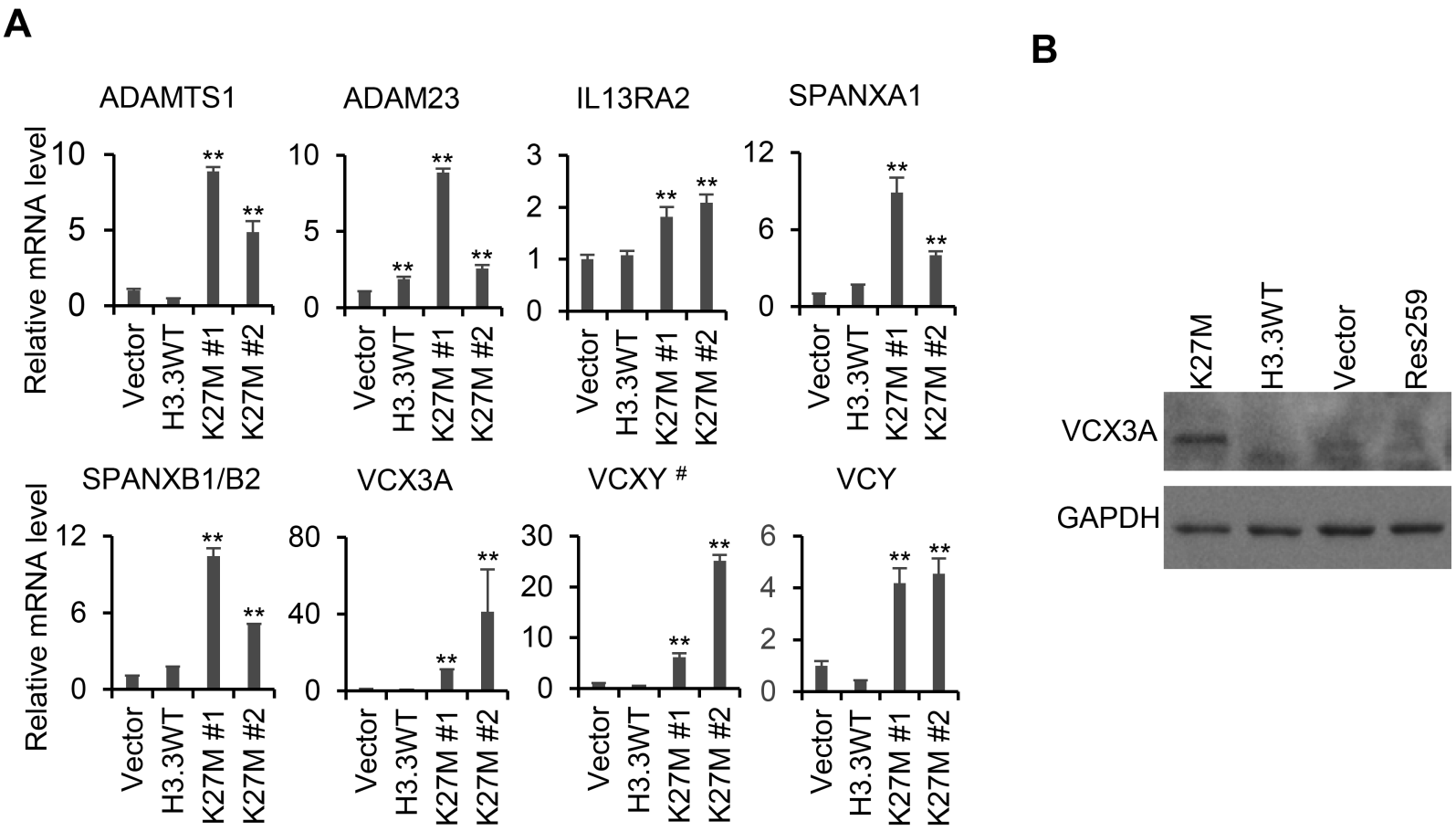
A
ADAMTS1
ADAM23
IL13RA2
SPANXA1
SPANXB1/B2
VCX3A
VCXY #
VCY
Relative mRNA level
Vector
H3.3WT
K27M #1
K27M #2
**
B
K27M
H3.3WT
Vector
Res259
VCX3A
GAPDH

Fig. 3

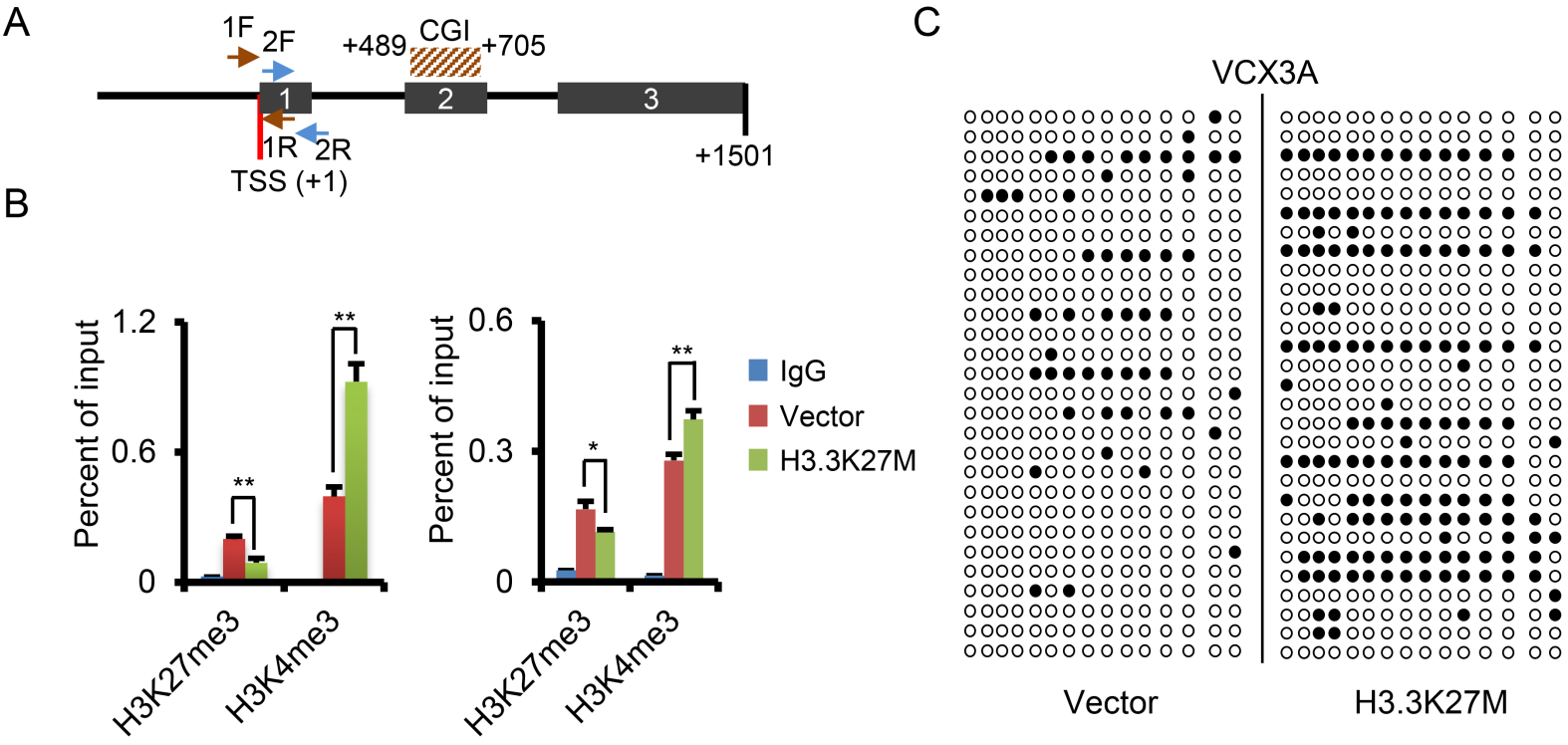
A
1F
2F
+489
CGI
+705
1
2
3
1R
2R
TSS (+1)
+1501
B
Percent of input
1.2
0.6
0
**
**
H3K27me3
H3K4me3
Percent of input
0.6
0.3
0
*
**
H3K27me3
H3K4me3
IgG
Vector
H3.3K27M
C
VCX3A
Vector
H3.3K27M

Fig. 4

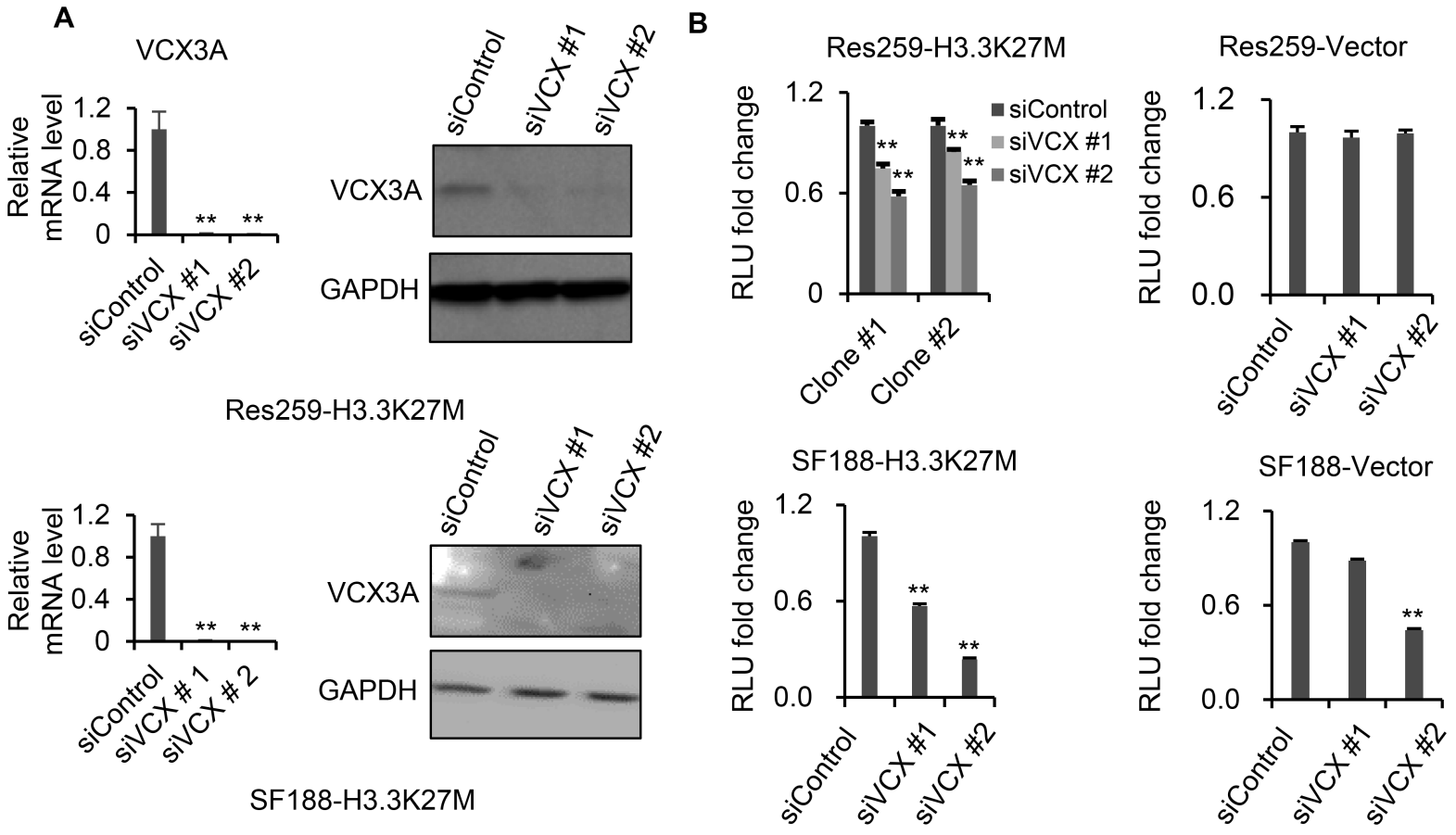
A
VCX3A
Relative mRNA level
1.2
0.8
0.4
0
**
**
siControl
siVCX #1
siVCX #2
siControl
siVCX #1
siVCX #2
VCX3A
GAPDH
Res259-H3.3K27M
SF188-H3.3K27M
B
Res259-H3.3K27M
Res259-Vector
SF188-H3.3K27M
SF188-Vector
RLU fold change
1.2
0.6
0.0
siControl
siVCX #1
siVCX #2
Clone #1
Clone #2

Fig. 5

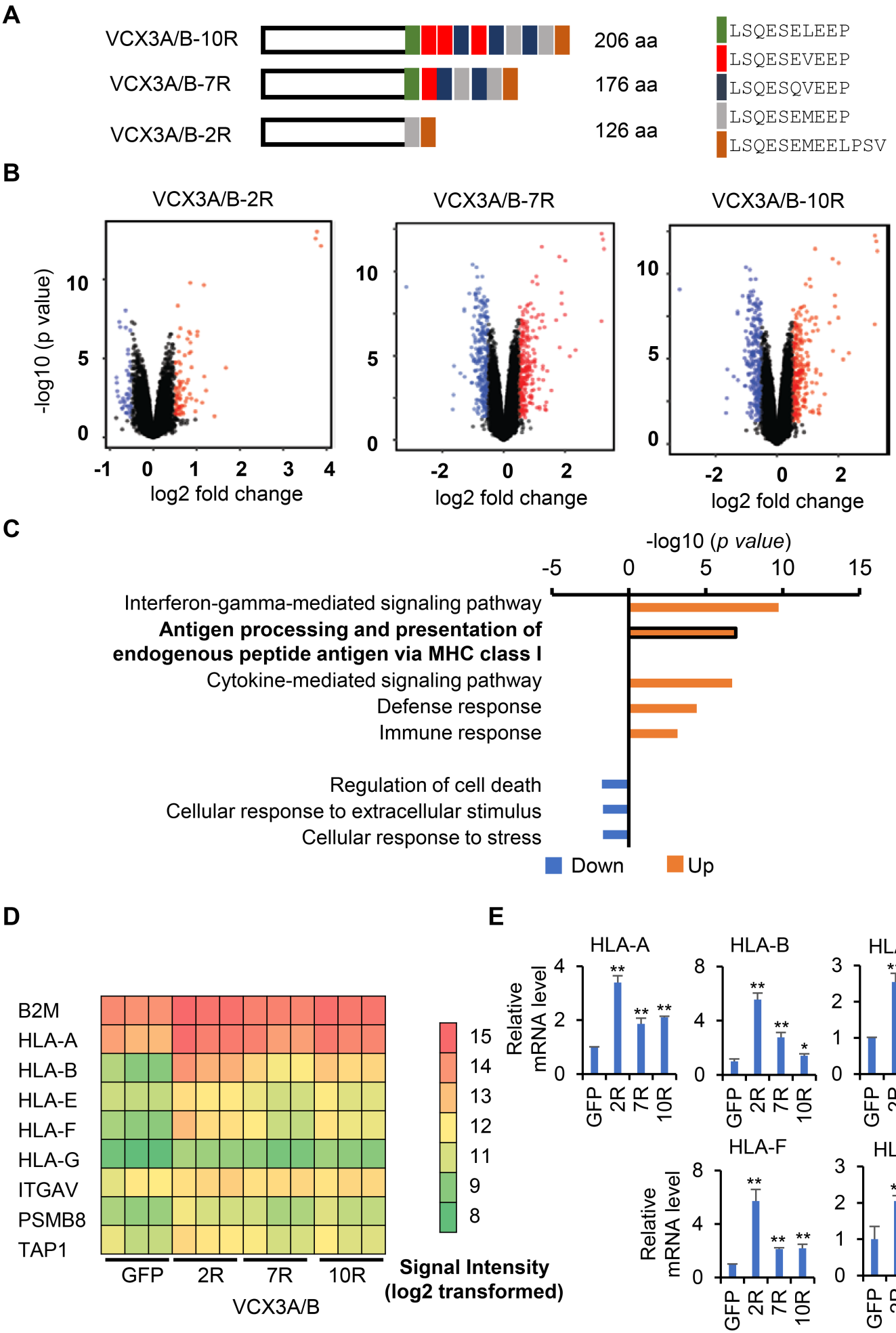
A
VCX3A/B-10R
VCX3A/B-7R
VCX3A/B-2R
206 aa
176 aa
126 aa
LSQESELEEP
LSQESEVEEP
LSQESQVEEP
LSQESEMEEP
LSQESEMEELPSV
B
VCX3A/B-2R
VCX3A/B-7R
VCX3A/B-10R
-log10 (p value)
log2 fold change
C
-log10 (p value)
Interferon-gamma-mediated signaling pathway
Antigen processing and presentation of endogenous peptide antigen via MHC class I
Cytokine-mediated signaling pathway
Defense response
Immune response
Regulation of cell death
Cellular response to extracellular stimulus
Cellular response to stress
Down
Up
D
B2M
HLA-A
HLA-B
HLA-E
HLA-F
HLA-G
ITGAV
PSMB8
TAP1
GFP
2R
7R
10R
VCX3A/B
Signal Intensity (log2 transformed)
E
HLA-A
HLA-B
HLA-E
HLA-F
HLA-G
Relative mRNA level
GFP
2R
7R
10R

Fig. 6

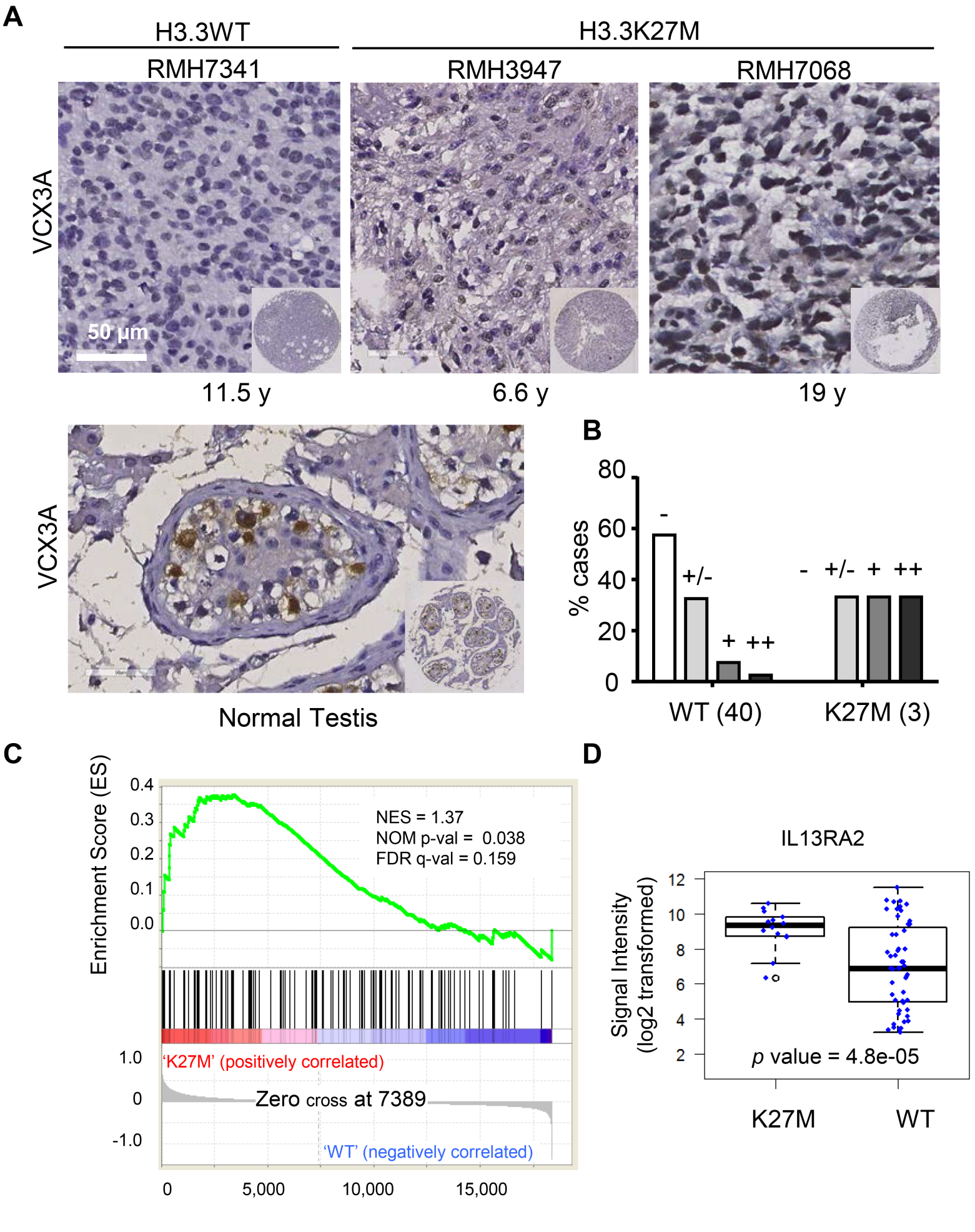
A
H3.3WT
H3.3K27M
RMH7341
RMH3947
RMH7068
VCX3A
50 µm
11.5 y
6.6 y
19 y
VCX3A
Normal Testis
B
% cases
80
60
40
20
0
-
+/-
+
++
- +/- + ++
WT (40)
K27M (3)
C
Enrichment Score (ES)
0.4
0.3
0.2
0.1
0.0
NES = 1.37
NOM p-val = 0.038
FDR q-val = 0.159
1.0
0
-1.0
'K27M' (positively correlated)
Zero cross at 7389
'WT' (negatively correlated)
0
5,000
10,000
15,000
D
IL13RA2
Signal Intensity
(log2 transformed)
12
10
8
6
4
2
p value = 4.8e-05
K27M
WT

Fig. 7